On the estimation of structural admittances from acoustic measurement using a dynamic substructuring approach

Domen Ocepek[a], Miha Kodrič[a], Gregor Čepon[a,*], Miha Boltežar[a]

[a] *University of Ljubljana, Faculty of Mechanical Engineering, Aškerčeva 6, 1000 Ljubljana, Slovenia*

Cite as:
Domen Ocepek, Miha Kodrič, Gregor Čepon and Miha Boltežar,
On the estimation of structural admittances from acoustic measurement using a dynamic substructuring approach,
Applied Acoustics, 2021, https://doi.org/10.1016/j.apacoust.2021.108115

Abstract

A reconstructed displacement field using near-field acoustic holography (NAH) serves as an alternative to conventional measurement methods when it comes to obtaining the high-resolution vibration response of a structure. The method is highly applicable as it enables direct, non-contact measurement of the 3D structural response based on a single acoustic measurement. Although useful, the method's ill-posed nature limits its use in the field of structural dynamics. This problem can be effectively addressed by using regularization and/or field-separation techniques that can attenuate the noise and the presence of external acoustic sources. All these methods rely on the measurement of acoustic quantities; therefore, the reconstruction of structural admittances is based solely on the evaluation of the hologram(s). This article proposes an alternative approach to improving the accuracy of NAH-based structural admittances by integrating them with a few discrete response measurement on the structure itself. The formulation relies on the mixing of the high-resolution NAH measurement with accurate discrete measurements (e.g., accelerometer or laser vibrometer) using dynamic substructuring techniques. The proposed hybrid approach is a very

*Corresponding author: gregor.cepon@fs.uni-lj.si, +386 1 4771 229, fax:+386 1 2518 567

powerful modeling methodology that can integrate high-resolution spatial measurements using NAH with the accuracy and consistency provided by precise translation discrete measurements. In order to mix two experimental response models System Equivalent Model Mixing (SEMM) method is proposed. An experimental case study on a T-shaped structure demonstrates the robustness and improved accuracy of the estimated structural admittances compared to the plain NAH formulation.

Keywords: Acoustic measurement, Near-field acoustic holography, Dynamic substructuring, System equivalent model mixing, Hybrid model

---

1. Introduction

Displacement identification based on acoustic measurement offers an alternative to traditional measurement methods such as accelerometers, laser vibrometry and optical methods. While accurate, acceleration transducers allow the user to acquire the dynamic information only at a discrete point [1], and even a relatively small mass of the accelerometer can impose a problem, especially with lightweight structures [2]. Non-contact methods such as laser vibrometry can be used to measure the dynamic response of the structure at a discrete locations. Laser scanning vibrometer can be applied to deduce out-of-plane vibrations, however, acquiring in-plane response requires multiple vibrometers [3]. Optical measurement offer a spatially dense measurement, although the estimated displacement from high speed camera generally exhibit relatively high levels of noise [4].

The structural response measurement using near-field acoustic holography (NAH) [5] relies on the acoustic pressure measurement called a hologram. This non-contact method is based on the source information captured in the near field of an acoustic source. A fine grid of microphone positions enables a spatially dense measurement and with this the possibility to obtain a high-resolution and accurate 3D structural response. In contrast to laser vibrometery or high-speed camera measurement, the 3D reconstruction can be obtained directly from the acoustic measurement performed in a single plane, eliminating the need for multiple measurement systems arranged in appropriate configuration to reconstruct the 3D displacement field. With clear advantages of acoustic holography measurement, the NAH based measurements were used for application in the automotive industry [6], health monitoring [7] and modal parameter identification [8].

Original NAH [5] is based on discrete Fourier transform (DFT) and imposes certain limitations on the source identification. The method enables the measurement of holograms obtained at a constant distance from the planar-shaped emitting surface, assuming a source-free region. In order to accurately reconstruct the normal surface velocity, a pressure-field measurement over a complete area is required so that the sound field falls to negligible levels outside the measurement aperture. The problems associated with small measurement areas can be addressed with a set of the patch NAH [9, 10] methods, such as the statistically optimized NAH (SONAH) [11] or equivalent sources model (ESM) [12] that avoid truncation errors introduced by the DFT. Other methods that solve Helmholtz integral equation such as the boundary element method (BEM) [13], Helmholtz equation least-squares (HELS) method [14] and the hybrid NAH [15] can be used to deduce the acoustic pressure radiating from arbitrarily shaped surfaces. SONAH methodology is appealing to use when dealing with planar acoustic sources as there is no need for measurement aperture to exceed dimensions of the source. SONAH also exploits benefits of simple application of Tikhonov regularization [16], suppressing measurement errors in order to obtain meaningful solution.

Taking into account all the variations and improvements of the presented NAH methods, the overall accuracy of the method is still strongly influenced by the measurement environment and the presence of background noise. Therefore, NAH is typically limited to anechoic environments where any interfering sources are eliminated. In order to assess the sound field radiated by the source of interest in noisy environments, field-separation techniques are commonly used. These methods apply separation of the measured sound field into the incoming and outgoing sound field. The former represents the sound approaching from the environment, while the latter, coming from the target source, is a combination of the free-field generated by the source surface and the scattering field due to the incoming wave. Particularly at high frequencies [17] or in small cavities [18], the scattering field is not to be neglected. In order to recover free-field conditions, field-separation methods (FSM) based on DFT NAH [19–21], BEM [22, 23], ESM [17, 24] and SONAH [25, 26] were developed. The majority of FSMs rely on measurements of the acoustic pressure in two closely spaced planes or combined measurements of the acoustic pressure and the particle velocity.

This paper presents an alternative approach to improving the consistency of the structural admittances obtained from the NAH. In contrast to regularization and/or field-separation techniques, which rely on the measurement of acoustic quantities, here the estimation of structural admittances is carried out by including the discrete measurement of the response on the structure itself. The methodology proposes the integration of the structural response model of the SONAH measurement with precise discrete measurements (e.g., accelerometer or laser vibrometer) in a few discrete points using dynamic substructuring (DS) techniques [27]. The method can be referred to as hybrid and therefore represents a very powerful modeling methodology that can integrate high-resolution spatial measurements using NAH with the accuracy and consistency provided by precise translation discrete measurements. The hybrid model is established using the recently developed System Equivalent Model Mixing (SEMM) method [28, 29]. With SEMM, different dynamic models of the same system can be mixed into a single hybrid model using the Lagrange-multiplier frequency-based substructuring (LM FBS) method [27, 30]. Hybrid model follows the dynamic behavior of a precise master model that is expanded to the all degrees of freedom (DoFs) of an equivalent slave model. Application of SEMM comprises the expansion of the experimental dynamics to the unmeasurable DoFs for use in coupling and decoupling processes [31], identification of inconsistent measurements in FBS [32, 33], and improving the accuracy of the experimental response models [34]. Some practical considerations for the successful application of SEMM were given in [35]. When a modal analysis is performed using NAH measurements, typically one excitation point is proposed [8]. Therefore, two experimental response models with only one driving-point measurement are mixed using the fully extended SEMM formulation. To demonstrate the accuracy and efficiency of the proposed technique, an experimental case study on a T-shaped structure is presented. It is clear that the hybrid approach offers a more consistent measurement of the structural response, especially with regards to the amplitude in the resonance regions. In addition, it can effectively address the issues associated with any microphone array misalignment. Finally, it was shown that the hybrid formulation can eliminate the external background acoustic sources from the structural response of the system.

The paper is organized as follows. The following section summarizes the basic theory of SONAH and dynamic substructuring with a focus on the LM FBS and SEMM methods. Section 3 presents a proposed hybrid approach for an improved estimation of the FRFs. Section 4 presents an experimental case study, followed by conclusions in the final section.

2. Theoretical background

2.1. Basic theory of SONAH

SONAH method makes it possible to reconstruct the normal surface velocity from a measurement on a near concentric surface. The sound pressure at arbitrary estimation position $\boldsymbol{r} = (x, y, z)$ above the source is reconstructed as a weighted sum of sound pressures, measured at N positions in the hologram plane, $\boldsymbol{r}_\mathrm{h} = (x_\mathrm{h}, y_\mathrm{h}, z_\mathrm{h})$:

$$p(\boldsymbol{r}) \approx \sum_{n=1}^{N} c_n(\boldsymbol{r}) p(\boldsymbol{r}_\mathrm{h}) = \boldsymbol{p}^\mathrm{T}(\boldsymbol{r}_\mathrm{h}) \boldsymbol{c}(\boldsymbol{r}). \tag{1}$$

Superscript T denotes that the vector $\boldsymbol{p}(\boldsymbol{r}_\mathrm{h})$ is transposed. Vector $\boldsymbol{c}(\boldsymbol{r})$ can be referred to as a transfer vector and is dependent on the geometry of microphone array and the estimation position $\boldsymbol{r}$:

$$\boldsymbol{c}(\boldsymbol{r}) = \left(\mathbf{A}^\mathrm{H}\mathbf{A} + \varepsilon\mathbf{I}\right)^{-1} \mathbf{A}^\mathrm{H} \boldsymbol{\alpha}(\boldsymbol{r}), \tag{2}$$

where $\mathbf{I}$ is the identity matrix, ε is the positive regularization parameter, based on Tikhonov regularization, and superscript H denotes Hermitian transpose. $\mathbf{A}^{\mathrm{H}}\mathbf{A}$ is a matrix of cross correlations between the measurement points and $\mathbf{A}^{\mathrm{H}}\boldsymbol{\alpha}(\boldsymbol{r})$ is a vector of cross correlations between measurement points and estimation position $\boldsymbol{r}$. Matrix $\mathbf{A}$ contains elementary wave functions evaluated at the hologram surface, while vector $\boldsymbol{\alpha}(\boldsymbol{r})$ consists of elementary wave functions evaluated at the estimation position $\boldsymbol{r}$. Considering infinite set of propagating and evanescent elementary wave functions, elements of $\mathbf{A}^{\mathrm{H}}\mathbf{A}$ and $\mathbf{A}^{\mathrm{H}}\boldsymbol{\alpha}(\boldsymbol{r})$ can be evaluated using one dimension integrals as described in [11].

A particle velocity vector $\boldsymbol{u}_\chi$ ($\chi = x,\ y,\ z$) can be obtained based on the Euler's equation of motion at the arbitrary estimation position $\boldsymbol{r}$ as:

$$\boldsymbol{u}_\chi(\boldsymbol{r}) = \frac{-1}{\mathrm{j}\omega\rho}\frac{\partial p(\boldsymbol{r})}{\partial \chi} = \frac{-1}{\mathrm{j}\omega\rho}\boldsymbol{p}^{\mathrm{T}}(\boldsymbol{r}_{\mathrm{h}})\left(\mathbf{A}^{\mathrm{H}}\mathbf{A} + \varepsilon\mathbf{I}\right)^{-1}\frac{\partial \mathbf{A}^{\mathrm{H}}\boldsymbol{\alpha}(\boldsymbol{r})}{\partial \chi}. \tag{3}$$

2.2. System Equivalent Model Mixing (SEMM)

The SEMM method was first introduced by Klaassen et al. [28] and is developed using Lagrange multiplier frequency-based substructuring (LM FBS) methodology [27]. This method allows the mixing of frequency-based models, either of a numerical or an experimental nature, to build a hybrid dynamic structural model of a given component.

First, a short recap of the LM FBS method theory is summarized according to [27]. To take into account all n subsystem, the integration of all the local matrices into the block-diagonal form is performed. The equation of motion considering all the subsystems in the frequency domain can be written as:[1]

$$\boldsymbol{u} = \mathbf{Y}\left(\boldsymbol{f} + \boldsymbol{g}\right),\ \text{where: } \mathbf{Y} = \begin{bmatrix} \mathbf{Y}^1 & & \\ & \ddots & \\ & & \mathbf{Y}^n \end{bmatrix},\ \boldsymbol{u} = \begin{bmatrix} \boldsymbol{u}^1 \\ \vdots \\ \boldsymbol{u}^n \end{bmatrix},\ \boldsymbol{f} = \begin{bmatrix} \boldsymbol{f}^1 \\ \vdots \\ \boldsymbol{f}^n \end{bmatrix},\ \boldsymbol{g} = \begin{bmatrix} \boldsymbol{g}^1 \\ \vdots \\ \boldsymbol{g}^n \end{bmatrix}. \tag{4}$$

[1] An explicit dependency on frequency is omitted to improve the readability of the notation, as will be the case for the remainder of the paper.

The vector $\boldsymbol{u}$ represents responses in all DoFs to the external force vector $\boldsymbol{f}$, and $\boldsymbol{g}$ is the vector of the connectivity forces at the interface to ensure equilibrium conditions. The matrix $\mathbf{Y}$ presents the block-diagonal admittance matrix of all the considered subsystems. The compatibility conditions are given with the signed Boolean matrix $\mathbf{B}$ (Eq. (5)), which ensures that the coupled structures have the same displacements at the interface DoFs. In addition to the compatibility conditions, the equilibrium conditions (Eq. (6)) must also be introduced by the interface forces in the form of a Lagrange multipliers vector $\boldsymbol{\lambda}$:

$$\mathbf{B}\,\boldsymbol{u} = \mathbf{0}, \tag{5}$$

$$\boldsymbol{g} = -\mathbf{B}^{\mathrm{T}}\boldsymbol{\lambda}. \tag{6}$$

After considering the equilibrium and compatibility conditions in Eq. (4) and eliminating the Lagrange-multipliers vector $\boldsymbol{\lambda}$, the response of the coupled structure can be written as:

$$\boldsymbol{u} = \tilde{\mathbf{Y}}\,\boldsymbol{f} = \left[\mathbf{Y} - \mathbf{Y}\,\mathbf{B}^{\mathrm{T}}\left(\mathbf{B}\,\mathbf{Y}\,\mathbf{B}^{\mathrm{T}}\right)^{-1}\mathbf{B}\,\mathbf{Y}\right]\boldsymbol{f}. \tag{7}$$

Eq. (7) is a single-line equation of the LM FBS to couple models and represents the basic formulation for the entire SEMM theory.

The basic idea of the SEMM method is shown in Fig. 1. The method is based on the parent model (Fig. 1a), which provides the extensive set of DoFs. The actual dynamic properties are provided by the overlay model (Fig. 1b). To form the final hybrid model (Fig. 1d) the dynamic properties of the parent model are decoupled by means of the removed model (Fig. 1c).

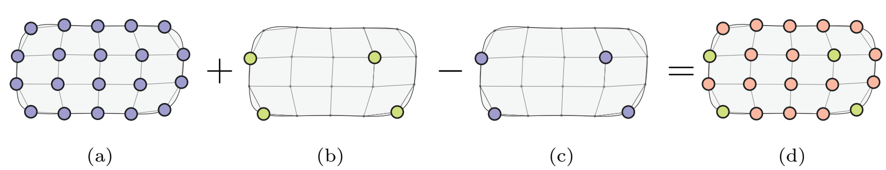

Figure 1: Equivalent models for the SEMM method; a) Parent model $\mathbf{Y}^{\mathrm{par}}$, b) Overlay model $\mathbf{Y}^{\mathrm{ov}}$, c) Removed model $\mathbf{Y}^{\mathrm{rem}}$, d) Hybrid model $\mathbf{Y}^{\mathrm{SEMM}}$.

The method uses a substructuring approach to expand the dynamic response model in an overlay model $\mathbf{Y}_{\mathrm{ov}}$ to the DoF space of a parent model $\mathbf{Y}_{\mathrm{par}}$. According to Eq. (4) the response of the hybrid model can be formulated as:

$$\boldsymbol{u} = \mathbf{Y}\left(\boldsymbol{f}+\boldsymbol{g}\right), \text{ where: } \mathbf{Y} \triangleq \begin{bmatrix} \mathbf{Y}^{\mathrm{par}} & & \\ & -\mathbf{Y}^{\mathrm{rem}} & \\ & & \mathbf{Y}^{\mathrm{ov}} \end{bmatrix}, \ \boldsymbol{f} = \begin{bmatrix} \boldsymbol{f}^{\mathrm{par}} \\ \boldsymbol{f}^{\mathrm{rem}} \\ \boldsymbol{f}^{\mathrm{ov}} \end{bmatrix}, \ \boldsymbol{g} = \begin{bmatrix} \boldsymbol{g}^{\mathrm{par}} \\ \boldsymbol{g}^{\mathrm{rem}} \\ \boldsymbol{g}^{\mathrm{ov}} \end{bmatrix}. \tag{8}$$

The entire DoF set of the parent model is divided into the internal (i) and boundary (b) DoFs. The boundary DoFs must overlap with the overlay model to enable the coupling of the response model, while the internal DoFs of the parent model can be arbitrarily arranged. The equivalent models within the SEMM method are formulated as admittance matrices by separating the internal and boundary DoFs:

$$\mathbf{Y}^{\mathrm{par}} \triangleq \begin{bmatrix} \mathbf{Y}_{\mathrm{ii}} & \mathbf{Y}_{\mathrm{ib}} \\ \mathbf{Y}_{\mathrm{bi}} & \mathbf{Y}_{\mathrm{bb}} \end{bmatrix}^{\mathrm{par}}, \quad \mathbf{Y}^{\mathrm{ov}} \triangleq \begin{bmatrix} \mathbf{Y}_{\mathrm{bb}} \end{bmatrix}^{\mathrm{ov}}, \quad \mathbf{Y}^{\mathrm{rem}} \triangleq \begin{bmatrix} \mathbf{Y}_{\mathrm{bb}} \end{bmatrix}^{\mathrm{par}}. \tag{9}$$

First, coupling of parent and overlay models projects dynamic properties of the latter on the full-span DoF provided by the parent model. To remove dynamics of the parent from the newly formed model, removed model (a condensed version of parent model defined in the boundary DoF) is decoupled, resulting in hybrid model following dynamic properties provided by the overlay model. Therefore, SEMM can be treated as an expansion method [28]. The compatibility and the equilibrium conditions (Eq. (5) and Eq. (6)) between the equivalent models must also be considered, where the signed Boolean matrix is defined as:

$$\mathbf{B} \triangleq \begin{bmatrix} \mathbf{B}^{\mathrm{par}} & \mathbf{B}^{\mathrm{rem}} & \mathbf{B}^{\mathrm{ov}} \end{bmatrix} = \left[\begin{array}{cc|c|c} \mathbf{0} & -\mathbf{I} & \mathbf{I} & \mathbf{0} \\ \mathbf{0} & \mathbf{0} & -\mathbf{I} & \mathbf{I} \end{array}\right]. \tag{10}$$

Following the LM FBS methodology and eliminating the Lagrange multipliers vector, the final equation is defined as:

$$\overline{\mathbf{Y}} = \mathbf{Y} - \mathbf{Y}\,\mathbf{B}^{\mathrm{T}}\left(\mathbf{B}\,\mathbf{Y}\,\mathbf{B}^{\mathrm{T}}\right)^{-1}\mathbf{B}\,\mathbf{Y}. \tag{11}$$

By considering the localization matrix [28], a reformulation to the primal notation is achieved. Finally, the single-line form of the basic SEMM method can be written using the primary admittance:

$$\mathbf{Y}^{\mathrm{SEMM}} = \mathbf{Y}^{\mathrm{par}} - \begin{bmatrix} \mathbf{Y}_{\mathrm{ib}} \\ \mathbf{Y}_{\mathrm{bb}} \end{bmatrix}^{\mathrm{par}} \left(\mathbf{Y}^{\mathrm{rem}}\right)^{-1} \left(\mathbf{Y}^{\mathrm{rem}} - \mathbf{Y}^{\mathrm{ov}}\right) \left(\mathbf{Y}^{\mathrm{rem}}\right)^{-1} \begin{bmatrix} \mathbf{Y}_{\mathrm{bi}} & \mathbf{Y}_{\mathrm{bb}} \end{bmatrix}^{\mathrm{par}}. \tag{12}$$

The basic SEMM method also has some extensions that increase its robustness [28]. Extension presented here removes any spurious peaks from the hybrid model in the frequency domain with an extension of the removed interface. If the removed interface is extended to all the internal DoFs, then the removed model has the following form:

$$\mathbf{Y}^{\mathrm{rem}} = \begin{bmatrix} \mathbf{Y}_{\mathrm{ii}} & \mathbf{Y}_{\mathrm{ib}} \\ \mathbf{Y}_{\mathrm{bi}} & \mathbf{Y}_{\mathrm{bb}} \end{bmatrix}^{\mathrm{par}}. \tag{13}$$

With extended interface removal of the parent dynamics from the hybrid model is improved. The final form of the fully extended SEMM method in a single-line notation is:

$$\mathbf{Y}^{\mathrm{SEMM}} = \mathbf{Y}^{\mathrm{par}} - \mathbf{Y}^{\mathrm{par}} \left(\begin{bmatrix} \mathbf{Y}_{\mathrm{bi}} & \mathbf{Y}_{\mathrm{bb}} \end{bmatrix}^{\mathrm{rem}} \right)^{+} \left(\mathbf{Y}^{\mathrm{rem}}_{\mathrm{bb}} - \mathbf{Y}^{\mathrm{ov}}\right) \left(\begin{bmatrix} \mathbf{Y}_{\mathrm{ib}} \\ \mathbf{Y}_{\mathrm{bb}} \end{bmatrix}^{\mathrm{rem}} \right)^{+} \mathbf{Y}^{\mathrm{par}}, \tag{14}$$

where superscript + denotes a pseudo-inverse.

3. Estimation of structural admittances from SONAH using SEMM

The hybrid formulation refers to the coupling of structural admittances from different domain measurements. It is well known that the accuracy of the NAH methods is strongly affected by the presence of background acoustic sources, reflective environments or inaccuracies in the position of the microphone array. These interferences affect the accuracy of the reconstructed structural admittances and are usually addressed by using extensions to the NAH formulation in the form of regularization and field-separation techniques. This paper proposes a hybrid methodology that aims to improve the consistency of reconstructed FRFs from the NAH method by integrating SONAH-based structural admittances with the discrete measurement on the structure itself. A proposed approach, which comprises a dynamic substructuring technique, can be summarized in four steps that are schematically presented in Fig. 2:

STEP 1: Identification of the experimental response model using the SONAH method. The structure is excited using a modal hammer or electrodynamic shaker in a selected set E of excitation points. The acoustic pressure is measured using a microphone array at N discrete points that are located within the area of the vibrating structure. Eq. (3) is then used to deduce the vibrational response of the structure. In order to attenuate the measurement errors, the regularization of the inverse solution is performed. Appropriate regularization parameter ε is determined using L-curve criterion [16]. With vibrational response reconstructed, frequency response functions (FRFs) are then calculated for N DoFs. In order to improve the signal-to-noise ratio, it makes sense to carry out several measurements and to perform averaging.

STEP 2: Structural admittances obtained by the SONAH measurement are assembled in the form of an admittance matrix, which presents the basis for the evaluation of the parent and the removed model. The parent and the removed model are, in accordance with a fully extended SEMM, defined as:

$$\mathbf{Y}^{\mathrm{par}} = \mathbf{Y}^{\mathrm{rem}} = \begin{bmatrix} \mathbf{Y}_{\mathrm{ii}} & \mathbf{Y}_{\mathrm{ib}} \\ \mathbf{Y}_{\mathrm{bi}} & \mathbf{Y}_{\mathrm{bb}} \end{bmatrix}_{\mathrm{SONAH}} \in \mathbb{C}^{N \times E}. \tag{15}$$

STEP 3: Identification of the overlay model based on the laser vibrometer measurement in the boundary DoFs. Care should be taken to ensure DoF of the overlay model coincide with the boundary DoF of the parent model, minimizing bias errors. The laser-based experimental response model is re-ordered in the form of an admittance matrix and serves as an overlay model:

$$\mathbf{Y}^{\mathrm{ov}} = \Big[\mathbf{Y}_{\mathrm{bb}}\Big]_{\mathrm{laser}} \in \mathbb{C}^{n\times e}, \;\text{where: } n \leq N \text{ and } e \leq E. \tag{16}$$

The laser vibrometer measurement introduces consistency to the proposed hybrid formulation, since the measurement is not affected by a noisy acoustical environment, as only the structural response is measured.

STEP 4: Mixing all three identified response models into a hybrid model using the fully extended SEMM method using Eq. (14). The dimensions of the hybrid admittance matrix are equal to:

$$\mathbf{Y}^{\mathrm{SEMM}} \in \mathbb{C}^{N\times E}. \tag{17}$$

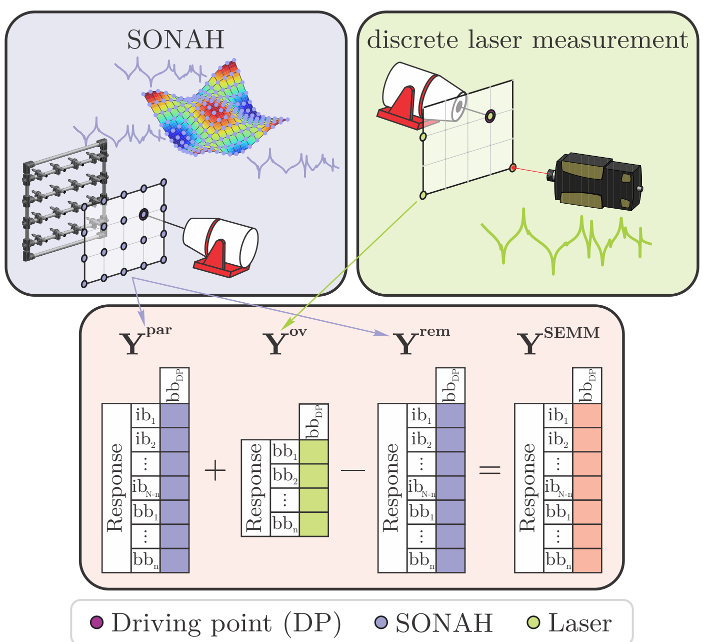

Figure 2: Schematic representation of the hybrid methodology for the structural admittances estimation from the SONAH using the fully extended SEMM method.

The typical use of the SEMM method involves mixing a numerical (parent) model with an experimental (overlay) model. Therefore, a full response model[2] for the parent model can always be obtained based on the numerical model. The disadvantage of using two experimental models as the input dynamics for the SEMM is the practical inability to obtain a full response model for the parent model. Therefore, the parent model and, consequently, the removed model are of reduced size and the motion, not observed in the parent model, imposes a certain limitation to the presented method [34]. A decoupling step in SEMM is compromised, as not all dynamic properties of the parent model are fully removed from the DoFs of the hybrid model. In case of SONAH methodology this is common due to limited controllability of the interface DoF, which is a consequence of a limited number of excitation points. However, as the parent and overlay models are both of experimental nature and observe similar dynamic behavior, this is proven not to be problematic and the hybrid model predicts overall dynamic response with sufficient accuracy. Experiment, presented later in this paper, investigates a limit case with only one driving point used (depicted in Fig. 2). With extension of the measurement to the several driving points, even more consistent hybrid models can be obtained. Quality of the decoupling step can be additionally validated using Interface Completeness Criterion (ICC) [36, 37] in order to ensure sufficient interface description.

It should be emphasized here that there are more advanced NAH formulations [12, 13] and already-established practices to address the problems with the presence of the external sound sources and other similar disturbances [25, 26]. Here, the idea is to demonstrate the possibility of integrating the discrete measurement performed on the structure with the high-resolution SONAH measurement using the substructuring approach. Since the formulation relies on the mixing of the structural admittances, it can be applied to all variations and improvements of the NAH formulations, such as DFT NAH, BEM, ESM, etc.

[2]When referring to a full response model, a full FRF admittance matrix is considered. The FRFs for each response DoF are obtained for the excitation at each separate DoF. Therefore, the full admittance matrix for each frequency is a square matrix.

4. Experiment

To demonstrate the efficiency and robustness of the proposed approach, an experimental case study on a T-shaped structure is presented. The approach characterization is based on a comparison of the structural admittances between the proposed SEMM-based SONAH and the classic, SONAH formulation. First, the accuracy and efficiency of the SEMM-based SONAH formulation is characterized, taking into account the ideal measurement conditions in the anechoic chamber. Second, the ability of the method to address the issues with the microphone-array misalignment problems when reconstructing structural admittances is presented. Finally, the robustness of the SEMM-based SONAH formulation is demonstrated in the ambient environment by eliminating the external sound sources from the structural response of the system.

4.1. Experimental Setup

An experiment was carried out on a test aluminium structure with the geometry and dimensions shown in Fig. 3. Free boundary conditions were applied using polyurethane foam blocks to support the plate facing the microphone

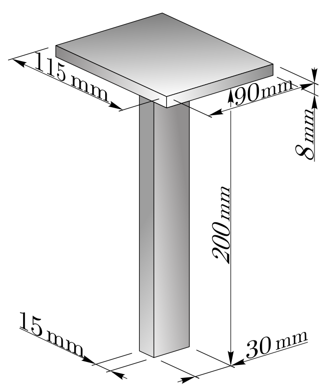

Figure 3: Test structure.

array. The structure was excited using a random noise signal with an electrodynamic shaker LDS V101 driven by a power amplifier. The excitation signal was generated using a Brüel&Kjær 2032 signal generator in a frequency band between 5 Hz (high-pass filter) and 3400 Hz. The excitation force was measured using a Dytran 1022V sensor. As the proposed methodology is also tested against external sources interfering with structural dynamics for its robustness, real-case interference was introduced by adding an external speaker emitting a sine wave at a frequency of 1800 Hz for the last experimental case (Fig. 4).

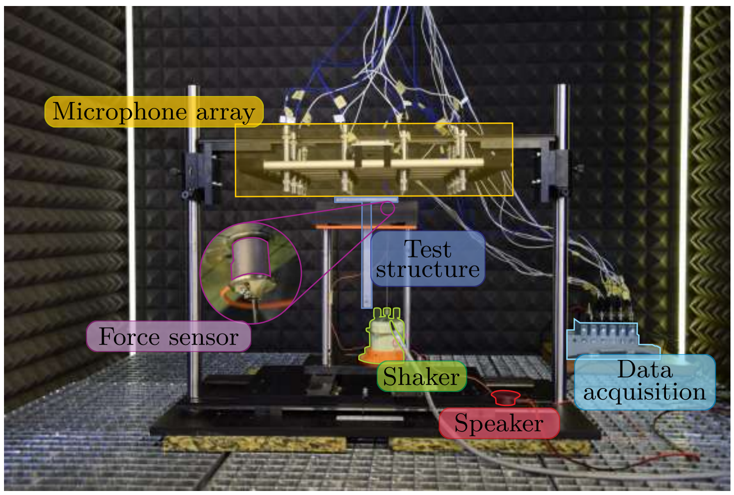

Figure 4: Experimental setup for the acquisition of experimental parent model using SONAH measurement.

As the acoustic measurements are highly subjected to background noise, an experimental (parent) model based on the SONAH methodology was measured in an anechoic chamber, as shown in Fig. 4. The microphone array, consisting of 16 PCB 378B02 microphones, was positioned parallel to the top surface of the structure at a distance of 12.5 mm. In order to improve spatial resolution of the acoustic measurement, spatial interspersing was used, translating the array in both directions and repeating measurements. A 20 s random noise signal was generated for excitation and stored in order to repeat equal excitation for each array position. Measurements were phase matched using measured excitation force. The acoustic response identified in 63 discrete points above the area of the vibrating structure, with a spacing of 12.5 mm between the microphones, was then selected from the full measured data set (of 1024 points). Ten measurement blocks, each duration of 1 s, were selected for the individual measurement point and and later used for FRF calculation and averaging. The frequency range of interest lies between 200 Hz and 3200 Hz, which contains the first six natural frequencies of the structure.

The second experimental model (overlay model) was acquired using the Polytec PDV-100 laser vibrometer. No changes were made with regards to the structure excitation and the boundary conditions. Responses were taken for selected discrete points on the top surface of the structure only. The experimental setup is shown in Fig. 5.

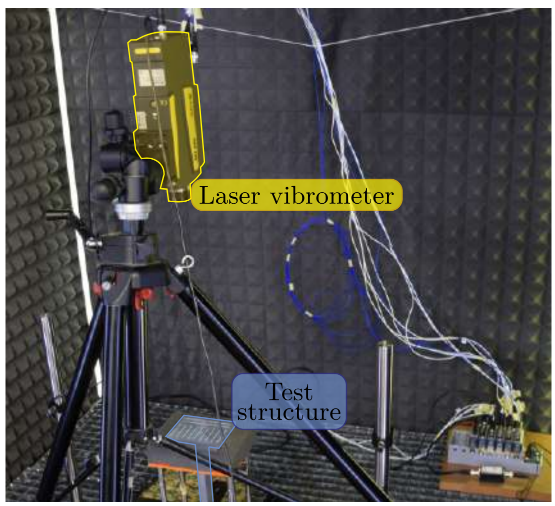

Figure 5: Experimental setup for the acquisition of experimental overlay model using laser vibrometer.

4.2. Equivalent models

The translational response of the plate in the z-direction was identified at $N = 63$ discrete points along the top surface of the plate and it represents the parent model.Since it is practically impossible and impractical to measure the full response model, only one driving point was proposed for both the parent and the overlay model. The response as the basis for the overlay model (laser measurement) was identified with three discrete points. Both models, together with the driving point, are schematically presented in Fig. 6.

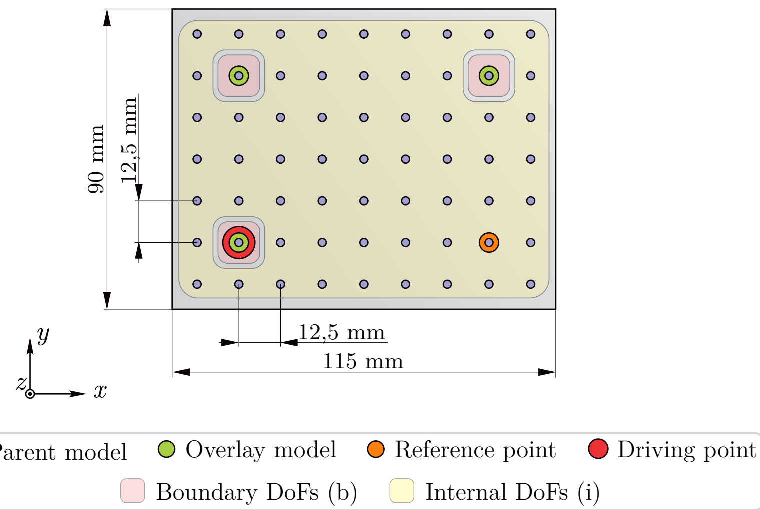

Figure 6: Schematic representation of the response models together with the reference and the driving point.

Parent and removed model are assembled accordingly to Eq. (15). With one driving point proposed, all excitation(s) are limited to a single boundary DoF ($E = 1$):

$$\mathbf{Y}^{\text{par}} = \mathbf{Y}^{\text{rem}} = \begin{bmatrix} \mathbf{Y}_{\text{ib}} \\ \mathbf{Y}_{\text{bb}} \end{bmatrix}_{\text{SONAH}} \in \mathbb{C}^{63\times 1}, \text{ where } \mathbf{Y}_{\text{ib}} \in \mathbb{C}^{60\times 1} \text{ and } \mathbf{Y}_{\text{bb}} \in \mathbb{C}^{3\times 1}. \tag{18}$$

Overlay model is assembled using Eq. (16) and consist of responses, taken in all three boundary DoFs ($n = 3$), while the structure is excited in proposed driving point ($e = 1$):

$$\mathbf{Y}^{\text{ov}} = \begin{bmatrix} \mathbf{Y}_{\text{bb}} \end{bmatrix}_{\text{laser}} \in \mathbb{C}^{3\times 1}. \tag{19}$$

Additional laser measurement was taken, but not considered in the overlay model or SEMM method in general. This measurement is treated as a reference for the further evaluation of the proposed hybrid approach. Measurement was taken at the internal DoF and as such provides a benchmark to assess the quality of the hybrid model and decoupling step in SEMM.

4.3. General evaluation of the proposed hybrid methodology

A comparison of the identified FRFs using the SONAH method and the proposed hybrid methodology with the reference measurement at hybrid model's internal DoF are shown in Fig. 7.

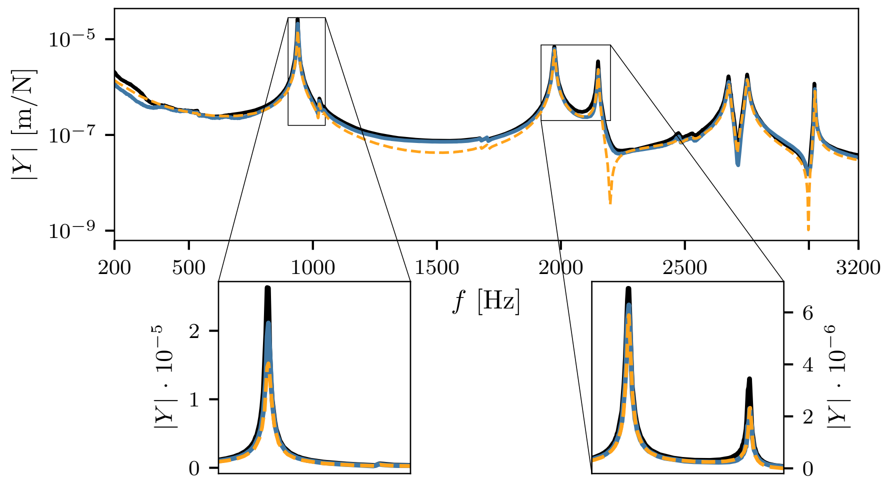

(a)

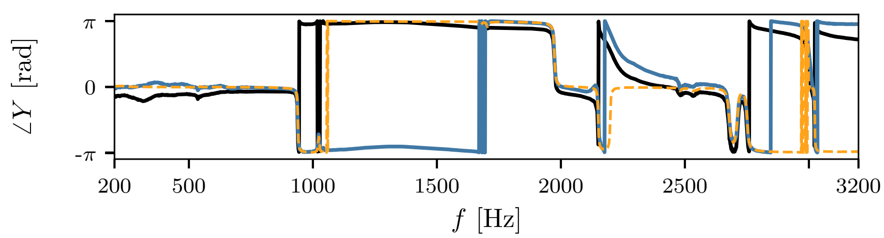

(b)

Figure 7: FRFs comparison in the reference point; a) Magnitude graph, b) Phase graph. (━) – SONAH, (━) – SEMM-SONAH, (- - -) – Reference measurement

Compared to the reference measurement, response identified using SONAH is slightly less accurate in the high-frequency range, which is in agreement with the observations presented in [38, 39]. The resonance peaks are well aligned in terms of the frequency, but differ in the amplitude of the response. Anti-resonance regions are poorly identified, due to the minor imperfections in microphone array and structure positioning.

By closely comparing the results of the SEMM-based SONAH formulation and the reference measurement, good agreement between the two is observed in the entire frequency range. Although, anti-resonance regions impose a problem to the hybrid methodology since they are poorly identified using SONAH. Due to the conflicting dynamics of the parent and the overlay model in these regions, decoupling step in SEMM is compromised and the hybrid model does not completely align with the reference. However, when compared to the SONAH measurement, estimation of anti-resonance regions is improved. The more accurate prediction of the hybrid formulation can be clearly observed by magnifying the resonance areas and plotting the FRFs on a linear scale (Fig. 7). At the resonance regions, consistency of the hybrid model's response amplitudes is improved when compared to the reference.

The improved accuracy of the hybrid model can be seen even more clearly if the FRFs are plotted on a Nyquist plot in the region of the resonance frequencies (Fig. 8). It can be concluded that the hybrid formulation proves to be more consistent since, in addition to a more precise evaluation of the amplitude, a more precise phase response can be observed.

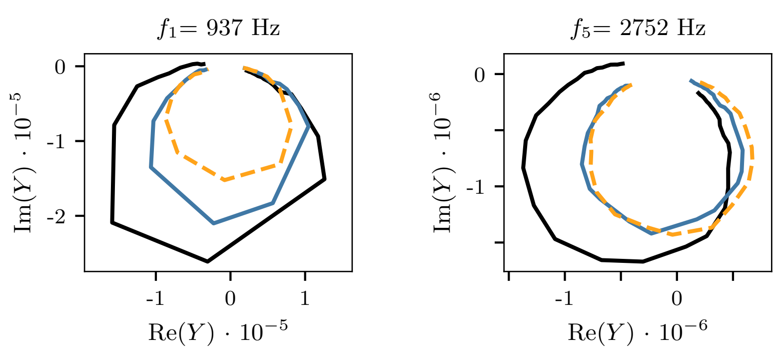

(a) (b)

Figure 8: FRFs comparison in the reference point presented on a Nyquist plot around selected natural frequencies; a) 1st natural frequency, b) 5th natural frequency.
(—) – SONAH, (—) – SEMM-SONAH, (- - -) – Reference measurement

However, in order to objectively assess the correlation between the FRFs, a more advanced criterion was proposed. The coherence criterion function [40] considers the comparison across the entire frequency range, both in terms of amplitude and phase. The frequency-dependent criterion indicates the correlation of the given FRF Y with a reference FRF Y_{ref}:

$$\text{coh}(f_k) = \frac{\Big(Y(f_k) + Y_{\text{ref}}(f_k)\Big)\Big(Y^*(f_k) + Y^*_{\text{ref}}(f_k)\Big)}{2\Big(Y^*(f_k)Y(f_k) + Y^*_{\text{ref}}(f_k)Y_{\text{ref}}(f_k)\Big)}, \tag{20}$$

where * stands for a complex conjugate. The coherence criterion is evaluated in the proximity of the resonant frequencies in the frequency range ($f_r - 20$ Hz, $f_r + 20$ Hz). The values close to one indicate a strong correlation between the compared FRFs. To obtain an overall correlation between the FRFs, an average coherence over the considered frequency range is introduced:

$$\overline{\text{coh}} = \frac{1}{K}\sum_{k}^{K} \text{coh}(f_k)\,. \tag{21}$$

The mean coherence values $\overline{\text{coh}}$ of the SONAH formulations for all the natural frequencies are shown in Fig. 9. In the low-frequency range, high coherence values are observed for both approaches. Here the hybrid model holds slightly higher values than the SONAH method. In the higher frequency range, the values of the coherence for the SONAH method decrease, while the FRFs of the hybrid model retain high values.

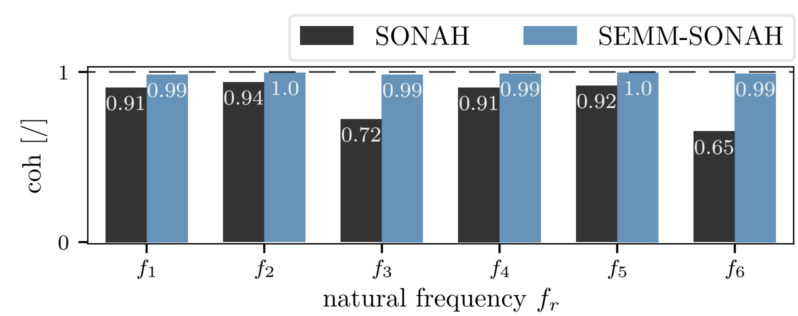

Figure 9: Comparison of the mean coherence value's $\overline{\text{coh}}$ for both SONAH approaches.

4.4. Analysis of the microphone array misalignment

The accuracy of the SONAH method is strongly influenced by the correct positioning of the microphone array with respect to the test structure. The microphone array misalignment during the SONAH measurement is reflected in an incorrectly determined hologram distance z_{h}. In order to simulate the microphone array misalignment, the measured hologram distance of $z_{\mathrm{h}} = 12.5$ mm was deliberately set to an erroneous value of $z_{\mathrm{h}} = 22$ mm during the SONAH evaluation. The comparisons of the reference and FRF obtained using the SONAH method are presented in Fig. 10.

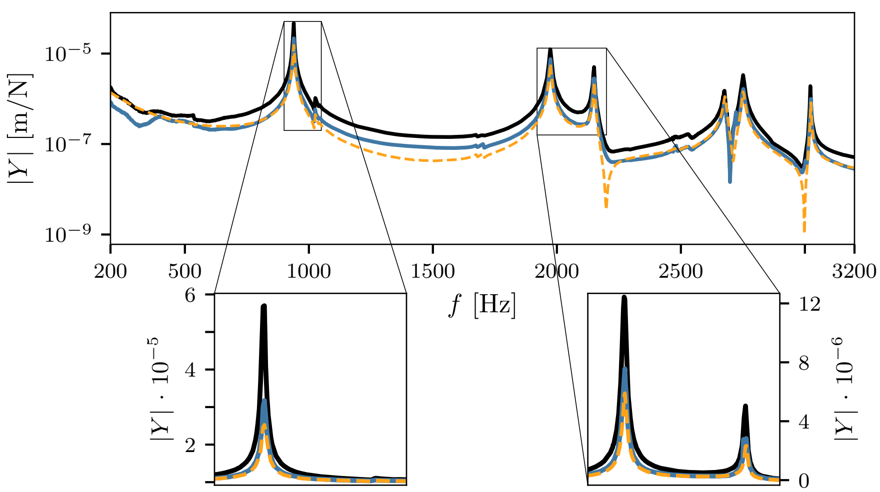

Figure 10: FRFs comparison at the reference point by considering an incorrect hologram distance.

(━) – SONAH, (━) – SEMM-SONAH, (- - -) – Reference measurement

Since the hologram distance was not correctly identified, the SONAH measurement in general predicts the shape of the FRF with sufficient accuracy, but the overall amplitudes are completely erroneous. With z_{h} larger than the actual offset, amplitudes of the SONAH based response strongly exceed the reference. However, hybrid approach can successfully address the issue with a microphone array misalignment. The hybrid formulation inherits the overall FRF shape from the SONAH measurement, and since the SONAH measurement is decoupled from the hybrid model, retaining dynamic response from an accurate laser measurement, the amplitudes in the entire frequency range correlate well with the reference measurement. In addition, both SONAH approaches are evaluated with a reference measurement using the coherence criterion (Fig. 11). It can be observed that a hybrid model results in far higher values compared to the SONAH method. The mixed hybrid approach, therefore, introduces a high degree of robustness into the SONAH formulation, as the precise positioning of the microphone array is not required.

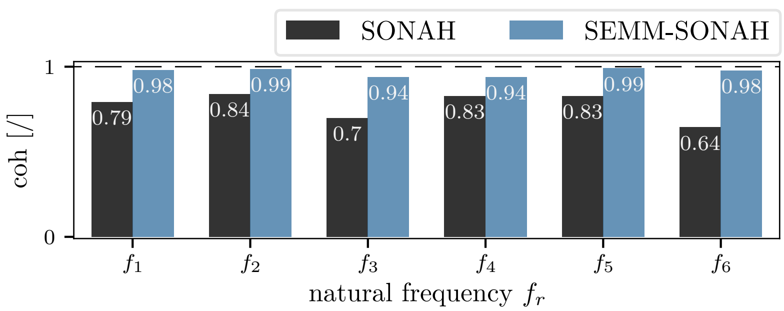

Figure 11: Comparison of the mean coherence values by considering an incorrect hologram distance.

4.5. The influence of external acoustic sources on the structural response of the system

In order to confirm the applicability and robustness of the proposed hybrid methodology, the entire experimental setup was positioned in the ambient environment. An additional external acoustic source was introduced using a simple loudspeaker tuned to a sine frequency of 1800 Hz. Using this experimental setup the SONAH and hybrid evaluations were performed. When using the SONAH methodology, the spurious peak due to the external acoustic source can be clearly identified at a frequency of 1800 Hz (Fig. 12). However, when using the proposed approach, this spurious acoustic source is effectively canceled out from the structural response of the system. This is shown more clearly from the Nyquist plot in the proximity of 1800 Hz (Fig. 13).

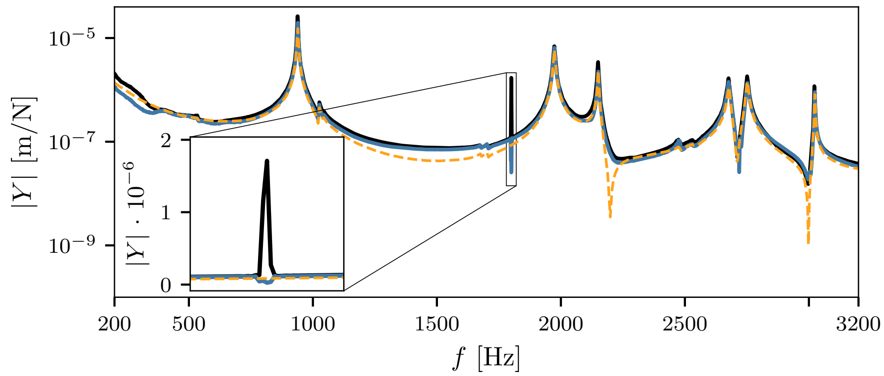

Figure 12: FRFs comparison at the reference point with the presence of an external acoustic source.
(━━) – SONAH, (━━) – SEMM-SONAH, (- - -) – Reference measurement

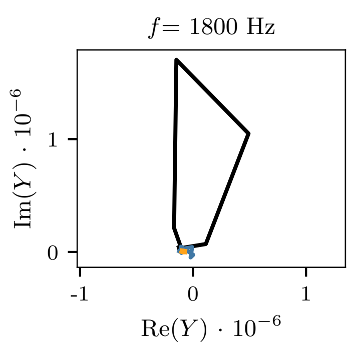

Figure 13: FRFs comparison at the reference point presented on a Nyquist plot around 1800 Hz in the presence of an external acoustic source.
(━━) – SONAH, (━━) – SEMM-SONAH, (- - -) – Reference measurement

Removal of this spurious dynamics originates from the definition of the removed model. The latter, originating from the parent model, includes this faulty dynamics. As the removed model is decoupled from the model resulting from coupling parent and overlay models, any dynamic behavior that is not involved in the overlay model is also decoupled from the hybrid model. Based on this presentation it is clear that the SEMM-based SONAH formulation makes it possible to eliminate the external tonal acoustic sources from the structural response.

5. Conclusion

In this work, dynamic substructuring techniques are introduced into the SONAH method to improve the consistency and accuracy of the identified structural response. The formulation can be considered as a pure hybrid approach, since structural admittances from different domain measurements (acoustic and velocity) are coupled to develop the hybrid formulation. It has been demonstrated that the structural FRFs identified directly by the SONAH method are subjected to imperfect measurement conditions, such as the presence of external acoustic sources, reflective surfaces and inaccuracies in the position of the microphone array. All of these disturbances can strongly influence the accuracy of the predicted structural response using the SONAH method.

The SEMM-based SONAH formulation enables a more accurate and consistent identification of the structural response by integrating the SONAH method with a precise, discrete laser measurement. The more consistent prediction of the proposed formulation is clearly observable with regards to the amplitude estimation in the resonance regions. It has also been shown that the hybrid formulation can effectively address the microphone-array misalignment problems and can completely eliminate external acoustic sources from the structural response of the system. The extension of NAH using SEMM aims to improve the consistency of the identified structural response in the form of an admittance matrix. The idea is applicable to all extensions and improvements to the NAH formulation, since it is based on the mixing of structural admittances.

Acknowledgements

The authors acknowledge partial financial support from the core research funding P2-0263 and the applied research project L2-1837, both financed by ARRS, the Slovenian research agency.

References

[1] M. Pogačar, T. Bregar, G. Čepon, M. Boltežar, Near-to-node modal identification using multiple related response models, Measurement (2020) 108793.

[2] C. Warren, C. Niezrecki, P. Avitabile, P. Pingle, Comparison of frf measurements and mode shapes determined using optically image based, laser, and accelerometer measurements, Mechanical Systems and Signal Processing 25 (6) (2011) 2191–2202.

[3] H. Khalil, D. Kim, J. Nam, K. Park, Accuracy and noise analyses of 3d vibration measurements using laser doppler vibrometer, Measurement 94 (2016) 883–892.

[4] J. Javh, J. Slavič, M. Boltežar, High frequency modal identification on noisy high-speed camera data, Mechanical Systems and Signal Processing 98 (2018) 344–351.

[5] J. D. Maynard, E. G. Williams, Y. Lee, Nearfield acoustic holography: I. theory of generalized holography and the development of nah, The Journal of the Acoustical Society of America 78 (1985) 1395–1413.

[6] F. Duvigneau, T. Luft, J. Hots, J. L. Verhey, H. Rottengruber, U. Gabbert, Thermo-acoustic performance of full engine encapsulations–a numerical, experimental and psychoacoustic study, Applied Acoustics 102 (2016) 79–87.

[7] W. Lu, W. Jiang, H. Wu, J. Hou, A fault diagnosis scheme of rolling element bearing based on near-field acoustic holography and gray level co-occurrence matrix, Journal of Sound and Vibration 331 (15) (2012) 3663–3674.

[8] A. van Velsen, E. Moers, I. L. Arteaga, H. Nijmeijer, Plate mode identification using modal analysis based on microphone array measurements, in: Proceedings of the EuroNoise conference, 2015.

[9] E. G. Williams, B. H. Houston, P. C. Herdic, Fast fourier transform and singular value decomposition formulations for patch nearfield acoustical holography, The Journal of the Acoustical Society of America 114 (2003) 1322–1333.

[10] M.-Y. Zhang, D.-Y. Hu, C. Yang, W. Shi, A.-H. Liao, An improvement of the generalized discrete fourier series based patch near-field acoustical holography, Applied Acoustics 173 107711.

[11] J. Hald, Basic theory and properties of statistically optimized near-field acoustical holography, The Journal of the Acoustical Society of America 125 (2009) 2105–2120.

[12] A. Sarkissian, Method of superposition applied to patch near-field acoustic holography, The Journal of the Acoustical Society of America 118 (2005) 671–678.

[13] M. R. Bai, Application of bem (boundary element method)-based acoustic holography to radiation analysis of sound sources with arbitrarily shaped geometries, The Journal of the Acoustical Society of America 92 (1992) 533–549.

[14] Z. Wang, S. F. Wu, Helmholtz equation–least-squares method for reconstructing the acoustic pressure field, The Journal of the Acoustical Society of America 102 (1997) 2020–2032.

[15] X. Zhao, S. Wu, Reconstruction of vibro-acoustic fields using hybrid nearfield acoustic holography, Journal of Sound and Vibration 282 (2005) 1183–1199.

[16] J. Gomes, P. C. Hansen, A study on regularization parameter choice in near-field acoustical holography, Journal of the Acoustical Society of America 123 (2008) 3385–3385.

[17] C.-X. Bi, J. Stuart Bolton, An equivalent source technique for recovering the free sound field in a noisy environment, The Journal of the Acoustical Society of America 131 (2012) 1260–1270.

[18] Y. Braikia, M. Melon, C. Langrenne, É. Bavu, A. Garcia, Evaluation of a separation method for source identification in small spaces, The Journal of the Acoustical Society of America 134 (2013) 323–331.

[19] M.-T. Cheng, J. A. Mann III, A. Pate, Wave-number domain separation of the incident and scattered sound field in cartesian and cylindrical coordinates, The Journal of the Acoustical Society of America 97 (1995) 2293–2303.

[20] D.-Y. Hu, C.-X. Bi, Y.-B. Zhang, L. Geng, Extension of planar nearfield acoustic holography for sound source identification in a noisy environment, Journal of Sound and Vibration 333 (2014) 6395–6404.

[21] E. Zea, I. L. Arteaga, Sound field separation for planar sources facing a parallel reflector, Applied Acoustics 149 (2019) 181–191.

[22] C. Langrenne, M. Melon, A. Garcia, Boundary element method for the acoustic characterization of a machine in bounded noisy environment, The Journal of the Acoustical Society of America 121 (2007) 2750–2757.

[23] C. Langrenne, M. Melon, A. Garcia, Measurement of confined acoustic sources using near-field acoustic holography, The Journal of the Acoustical Society of America 126 (2009) 1250–1256.

[24] E. Fernandez-Grande, F. Jacobsen, Q. Leclere, Sound field separation with sound pressure and particle velocity measurements, The Journal of the Acoustical Society of America 132 (2012) 3818–3825.

[25] F. Jacobsen, X. Chen, V. Jaud, A comparison of statistically optimized near field acoustic holography using single layer pressure-velocity measurements and using double layer pressure measurements, The Journal of the Acoustical Society of America 123 (2008) 1842–1845.

[26] E. Fernandez-Grande, F. Jacobsen, Sound field separation with a double layer velocity transducer array (l), The Journal of the Acoustical Society of America 130 (2011) 5–8.

[27] D. de Klerk, D. J. Rixen, S. Voormeeren, General framework for dynamic substructuring: history, review and classification of techniques, AIAA journal 46 (2008) 1169–1181.

[28] S. W. Klaassen, M. V. van der Seijs, D. de Klerk, System equivalent model mixing, Mechanical Systems and Signal Processing 105 (2018) 90–112.

[29] S. Klaassen, M. van der Seijs, Introducing semm: A novel method for hybrid modelling, in: Dynamics of Coupled Structures, Volume 4, 2018, pp. 117–125.

[30] D. de Klerk, D. J. Rixen, J. de Jong, The frequency based substructuring (fbs) method reformulated according to the dual domain decomposition method, in: Proceedings of the Fifteenth International Modal Analysis Conference, St. Louis, MO, 2006.

[31] Z. Saeed, S. W. Klaassen, C. M. Firrone, T. M. Berruti, D. J. Rixen, Experimental joint identification using system equivalent model mixing in a bladed-disk, Journal of Vibration and Acoustics (2020) 1–29.

[32] M. Kodrič, G. Čepon, M. Boltežar, Experimental framework for identifying inconsistent measurements in frequency-based substructuring, Mechanical Systems and Signal Processing 154 (2021) 107562.

[33] Z. Saeed, C. M. Firrone, T. M. Berruti, Joint identification through hybrid models improved by correlations, Journal of Sound and Vibration 494 115889.

[34] T. Bregar, K. Zaletelj, G. Čepon, J. Slavič, M. Boltežar, Full-field frf estimation from noisy high-speed-camera data using a dynamic substructuring approach, Mechanical Systems and Signal Processing 150 (2020) 107263.

[35] E. Pasma, S. Klaassen, L. Nieuwenhuijse, M. van der Seijs, D. Lennström, Application of system equivalent model mixing (SEMM) to model the structural dynamic properties of a complex vehicle component using numerical and experimental data, in: Proceedings of ISMA2018, 2018.

[36] J. Meggitt, A. Moorhouse, A. Elliott, On the problem of describing the coupling interface between sub-structures: An experimental test for 'completeness', in: Dynamics of Coupled Structures, Volume 4, Springer, 2018, pp. 171–182.

[37] J. Meggitt, A. Moorhouse, On the completeness of interface descriptions and the consistency of blocked forces obtained in situ, Mechanical Systems and Signal Processing 145 (2020) 106850.

[38] C. Pezerat, Q. Leclère, N. Totaro, M. Pachebat, Identification of vibration excitations from acoustic measurements using near field acoustic holography and the force analysis technique, Journal of sound and vibration 326 (2009) 540–556.

[39] K. Chelliah, G. Raman, R. T. Muehleisen, An experimental comparison of various methods of nearfield acoustic holography, Journal of Sound and Vibration 403 (2017) 21–37.

[40] A. Drozg, J. Rogelj, G. Čepon, M. Boltežar, On the performance of direct piezoelectric rotational accelerometers in experimental structural dynamics, Measurement 127 (2018) 292–298.